Mechanisms for Formation of a One-Dimensional Horizontal Anodic Aluminum Oxide Nanopore Array on a Si Substrate

Zhi Chen[z] and Hongguo Zhang

Department of Electrical and Computer Engineering and Center for Nanoscale Science and Engineering, University of Kentucky, Lexington, Kentucky 40506, USA

A simple theoretical model based on electric-field-assisted growth and dissolution of the barrier oxide has been proposed to understand the mechanisms for formation of a one-dimensional (1D) anodic aluminum oxide (AAO) nanopore array. It is shown that formation of a one-dimensional horizontal nanopore array is the natural result of the self-adjusting effect of anodic oxidation. Because the electric field for anodization is in parallel with an aluminum film, the porous structure is formed on the side of aluminum. When the thickness of an aluminum film approaches the size of a single cell, a single array of nanopores evolves after anodization in a steady state for sufficiently long time. Our experimental results support the theoretical model. A well-ordered one-dimensional nanopore array was obtained at 40 V in 0.3 M oxalic acid solution using the modified two-step anodization procedure.
© 2005 The Electrochemical Society. [DOI: 10.1149/1.2120347] All rights reserved.

Various carbon nanotube- and nanowire-based nanoscale electronic devices, such as field-effect transistors (FETs), single-electron transistors (SETs), metal-semiconductor diodes, rectifiers, and nanowire pumped lasers have been in the spotlight of nanoscale science and engineering due to their superior performance, such as unique electronic properties, strong mechanical strength, chemical and thermal stability.[1-6] However, most of these nanoscale devices were fabricated using scanning tunneling microscope (STM) and atomic force microscope (AFM), which are not suitable for large-scale manufacturing.[7,8] It is necessary to fabricate nanoscale devices in such a way that large-scale production is possible. Up to now, self-assembly processes appeared to be a promising approach.

Recently, research on nanoscale templates based on anodic aluminum oxide (AAO) inspired the nanoscale electronics' creative line. Due to the high aspect ratio ($\sim$1000) and high pore density of 10^{11} pores/cm^2, highly ordered and highly uniform AAO membranes and arrays are the most attractive self-assembly techniques. They are suitable for many technical applications in nanoscale electronics.[9-12] If an AAO template is built on a Si substrate, mature Si processing technologies can be used directly for fabrication of nanoelectronic devices.[13,14] The high level of ordering and uniformity of nanoscale device arrays on an AAO/Si substrate is more useful for areas such as data storage, field emission displays, and sensors. Fabrication of nanowire arrays using AAO templates such as metal wires (Bi, Ni), semiconductor wires (GaN, InGaAsN), and carbon nanotubes has been successfully demonstrated.[15-18] Although AAO nanotemplates have demonstrated potential for nanofabrication, it is still difficult to utilize them for fabrication of nanoelectronic devices and nano-electromechanical system. This is because nanopores in all the AAO templates are formed vertically on substrates in two dimensions (2D), not compatible with the mainstream planar processing technology. If an AAO template with a one-dimensional (1D) array of nanopores horizontally aligned on a substrate can be formed, it will have much broader applications in fabrication of nanoelectronic devices and nano-electromechanical systems.

In the past several decades, fabrication of 2D AAO nanopore arrays was studied extensively, and the correlation between the ordered nanoporous structure and the formation parameters was understood in great detail.[19-21] The porous structure consists of closely packed hexagonal cells with pores at the centers of the cells. The pore and cell sizes are uniquely correlated, depending on the formation parameters such as electrolyte composition, solution temperature, and applied voltage. In 1993, Masuda et al.[22] proposed a novel approach to fabricate an AAO template with a 1D array of nanopores using a sandwich structure of Al$_2$O$_3$/Al/glass. However, no follow-up research has ever been carried out, and the pore structures are hardly distinguishable in their SEM pictures.[22] In addition, in their process a thick Al$_2$O$_3$ film and a glass substrate are used, which are not compatible with the silicon integrated circuit processes. There are also concerns such as microcracks at interfaces and uniformity of pores and cells. Recently, we successfully fabricated a horizontal 1D AAO array based on the SiO$_2$/Al/SiO$_2$/Si structure using a modified two-step anodization process (see Fig. 1 for the schematic structure[23]).

In this paper, we first present a theoretical model to analyze the formation mechanisms for the 1D AAO array. We show theoretically why a single nanopore array is formed in the steady state due to the "self-adjusting effect." Then, we present experimental results in the initial and steady phases that are in agreement with our theoretical analysis.

Theoretical Model of Formation of a One-Dimensional Nanopore Array

Formation of porous structures.— In order to understand the formation of 1D horizontal arrays of nanopores, the evolution of 2D vertical AAO arrays and the key parameters will be described as follows.[19,24,25] The AAO arrays consist of three distinct layers: aluminum metal, a thin barrier oxide layer, and a relatively thick porous oxide layer (see Fig. 2). Initially, high current flows and oxide is formed rapidly. After a short time, current has decreased to a relatively low steady value and the barrier layer is completely formed. The barrier-layer thickness is dependent on the applied voltage at a rate of 14 Å/V.[19] After the barrier layer forms, there are two competing processes: oxide formation due to anodization, and dissolution due to corrosive acids. The oxide formation and dissolution reach a balance in a relatively short time. After that, anodic oxidation proceeds at a uniform rate. In the beginning, dissolution occurs at a single point. At this single point, the oxide thickness is reduced and current flows to repair the damage to the oxide layer (oxide formation). This increases the electrolyte temperature at this point, and more rapid dissolution of oxide occurs. Therefore, both the oxide formation and dissolution are assisted by electric field. This mechanism would perpetuate a pore once it is formed. As the current continues to flow through the single pore, additional oxide forms such that an oxide cell is created. Because the voltage and current fields originated from a point tend to be spherical, the advancing front of the oxide cell would be spherical. Because the pore is of finite size, the cell front will have the shape of spherical section somewhat less than a hemisphere (see Fig. 2). The thickness of the barrier layers would be less than the value corresponding to 14 Å/V
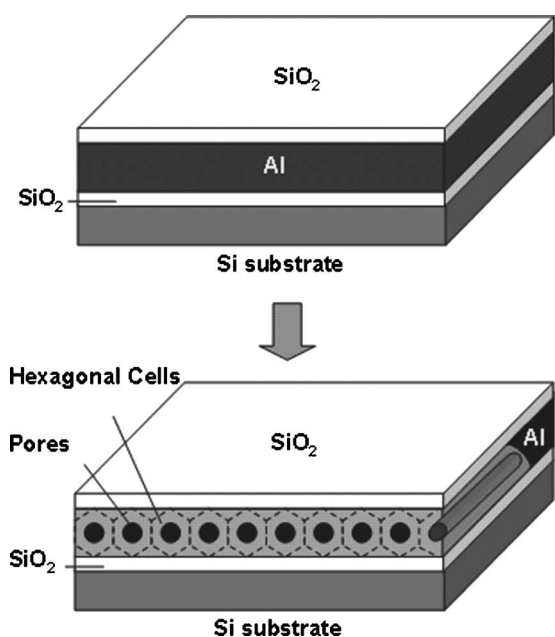
[z] E-mail: zhichen@engr.uky.edu

Figure 1. Schematic of a one-dimensional horizontal nanopore array.

because of more erosion of oxide in the pore by current flowing. Thus, as oxide is formed, a cylindrical cell which has a roughly hemispherical end and a central cylindrical pore will be formed, as shown in Fig. 2.[19]

Oxide cell and pore dimensions.— According to the contour of the cell base pattern, it is possible to determine the radius of curvature and the location of the center of curvature of the cell and the pore base (see Fig. 2b). These can be found by measuring the height and width of the pore base cross sections and using the formula[19]

$$R = \frac{H}{2} + \frac{W^2}{8H} \qquad [1]$$

where R is the radius of curvature, H is the height of the scallop, and W is the width of the scallop (cell size). The relationships between cell sizes, pore size, and forming voltage in various electrolytes can be determined by experiments. Pore size, wall thickness, and cell size apparently are determined by electrolytes and forming voltage.
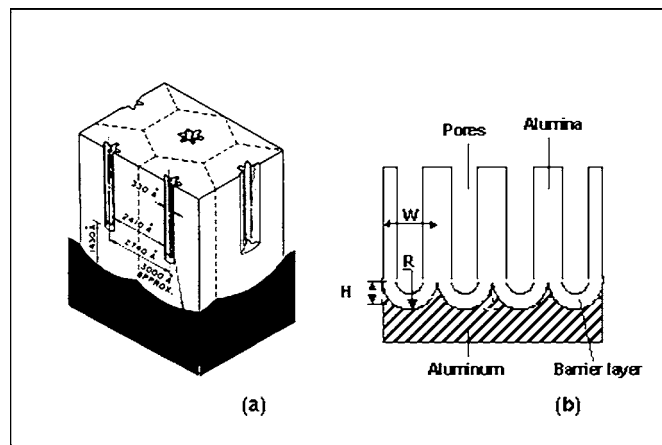
Table I. Pore diameter, wall thickness, and cell size of oxide coating for 2D AAO.

Electrolyte	Voltage V (V)	Pore diameter P (nm)	Wall thickness T (Å/V)	Cell size W (Å)
0.2 M Oxalic acid, 32°F	40	50	12.0	1460
0.3 M Sulfuric acid, 75°F	20	30	10.0	700
0.3 M Sulfuric acid, 75°F	10	15	9.0	330
0.3 M Sulfuric acid, 75°F	8	10	8.0	228

The relationship between cell size, wall thickness, pore size, and forming voltage is given by[26]

$$W = 2TV + P \qquad [2]$$

Where W is cell size, T is wall thickness in angstroms per volt, V is forming voltage, and P is pore diameter. The cell size W can be accurately determined depending on types of electrolytes and forming voltage V. The cell size is then used to determine the thickness of the aluminum film. Table I shows the pore diameter, wall thickness, and cell size in a variety of voltages for 2D AAO arrays.[19] If one wants to fabricate 1D array of nanopores, one may choose the thickness of the aluminum film close to the size of a single cell.

Effect of electric field on pore formation and self-adjusting effect.— Initially a barrier layer is formed. In a corrosive solution, right after the barrier layer formation, pores begin to be initiated. The pore and cell diameters and the barrier layer thickness increase and a number of major pores eventually propagate and certain incipient pores cease to function.[27,28] In the steady state, the field-assisted dissolution rate of oxide at the pore base (the solution/barrier-layer interface) equals the field-assisted growth rate of oxide at the cell base (the Al/barrier-layer boundary). As shown in Fig. 3a, the angle ω remains constant during the pore propagation deep into aluminum so that the scallop barrier layer forms. The rates of dissolution and oxidation depend on local electric field. Assuming that the current in a single cell is I passing from ab to cd, the current density $J(r)$ can be expressed as

$$J(r) = \frac{I}{(\omega/4\pi)4\pi r^2} = \frac{I}{\omega r^2} \qquad [3]$$

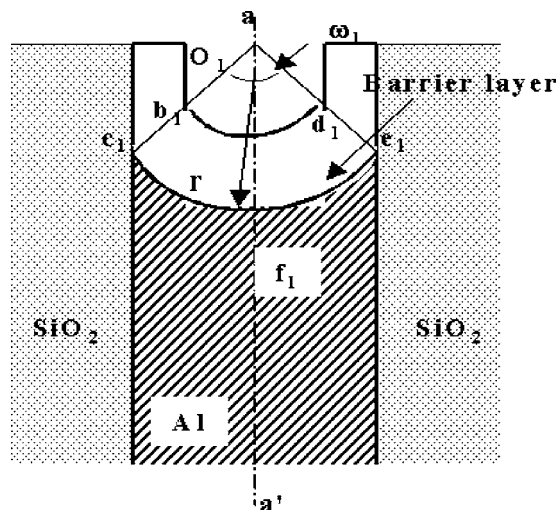and the electric field $E(r)$ inside the barrier layer is expressed as

Figure 2. (a) 3D structure of 120 V phosphoric acid coating constructed on cross section of cell base pattern [after Keller et al. (Ref. 19)]. (b) Schematic cross section of porous anodic aluminum oxid.

Figure 3. (a) The detailed schematic of the porous structure with scallop barrier layer in a regular nanotemplate. (b) The electric fields E_1 from cell 1 and E_2 from cell 2 reinforced the total field at point b.

$$E(r) = \frac{J}{\sigma} = \frac{I}{\sigma \omega r^2} \qquad [4]$$

where σ is the conductivity of the barrier layer. Because, in most cases, the voltage V across the barrier layer is constant, we have

$$\int_{r_a+b}^{r_a} E(r)dr = V \qquad [5]$$

Inserting Eq. 4 into Eq. 5, we obtained

$$I = \sigma \omega V \frac{r_a(r_a + b)}{b} \qquad [6]$$

Inserting Eq. 6 into Eq. 4, we have

$$E(r) = \frac{r_a(r_a + b)}{r^2} \frac{V}{b} \qquad [7]$$

Because of the geometric shape, the electric field increases toward the pore base, where the largest field is found. The electric field at the pore base can be calculated approximately from the barrier thickness rate (14 Å/V) and the applied voltage 40 V to yield 7.14 MV/cm. The electric field E_1 at the pore base and E_2 at the Al/barrier boundary are obtained from Eq. 7 with $r = r_a$ and $r = r_a + b$

$$E_1 = E(r_a) = \frac{(r_a + b)}{r_a} \frac{V}{b} \qquad [8]$$

$$E_2 = E(r_a + b) = \frac{r_a}{(r_a + b)} \frac{V}{b} \qquad [9]$$

From Eq. 8 and 9, it can be found that $E_2 < V/b < E_1$, where V/b is the field when the barrier layer is flat. The field-assisted dissolution rate of oxide at the pore base is proportional to E_1, and the field-assisted growth rate of oxide at the Al/barrier boundary is proportional to E_2.

In the steady state, the dissolution rate equals the oxidation rate, so that the pore formation propagates steadily with constant barrier thickness. Therefore, for certain voltage, there are equilibrium values of r_a and b, and thus the pore diameter P is also dependent on voltage V.

Self-adjusting effect.— During the steady state of anodization, the equilibrium values are maintained by the self-adjusting effect.[27] The self-adjusting effect is described as follows. For some reason, r_a decreases from its equilibrium value, causing E_1 in Eq. 8 to increase. This, in return, increases the dissolution rate (proportional to E_1), leading to a tendency to enlarge r_a. If r_a increases over its equilibrium value, E_1 will be reduced according to Eq. 8 so that the dissolution rate of oxide will also be reduced, resulting in a tendency to reduce r_a. Similar arguments can be applied to the self-adjusting of the barrier layer thickness b. The angle ω should also be constant in the steady state. As shown in Fig. 3b, when ω is too large, the electric field E_1 from cell 1 will partially cancel out E_2 from cell 2, so that the total field at point b is too small. This causes less lateral spread of the pore and the cell, and thus the angle ω will be reduced. In a limit case where $\omega = 180°$, the electric field E_1 from cell 1 will completely cancel out E_2 from cell 2, so that the total field is zero at point b. In this case, no oxidation and dissolution happen at point b, resulting in the stop of lateral spread of the cell and the pore. If the angle ω is too small, the total field at point b will be reinforced because of the sharp angle between E_1 and E_2. Thus, the enhanced field will enlarge the pore and the cell, leading to increase in ω. An equilibrium value of ω exists, which is 44.8° for 0.4 M oxalic acid.[27]

Confinement of cells and pores to a single array.— The direction of electric field determines the direction of nanopore arrays. Therefore, if the electric field is in parallel with aluminum, the porous structure may be formed on the side of aluminum as shown in
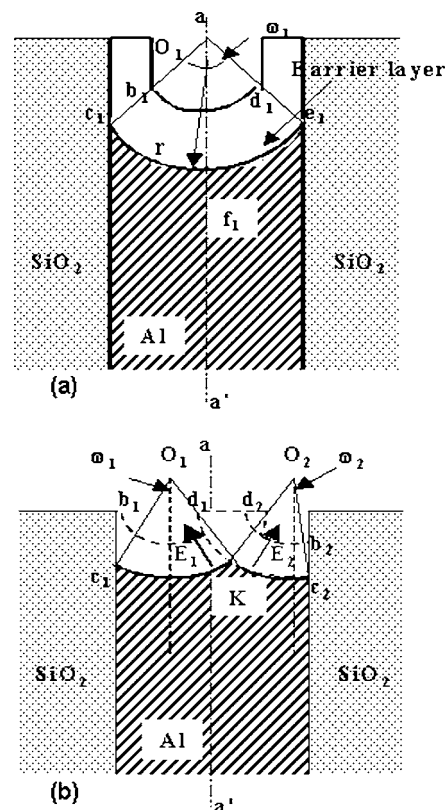
Figure 4. (a) Schematic of a single cell with a single pore formed in Al film of a single cell thickness sandwiched by two SiO$_2$ layers. The pore is formed from the side of the metal. (b) Schematic of an imagined case where two cells were cramped in the Al film that could, otherwise, only hold one cell. The effect of electric fields would push the two cells toward the central line aa', resulting in merge of two cells so that a single cell will be formed in equilibrium.

Fig. 1. By selecting the thickness of the aluminum film close to the cell size W, it is possible to form a single array of nanopores. As mentioned above, at a steady state the oxide formation and dissolution is balanced, depending on the electric field (accordingly, the voltage). As shown in Fig. 4a, a single cell and a single pore can be formed in a slab of aluminum sandwiched by two layers of SiO$_2$. One may argue that it might be possible to have two half-cells formed instead of a single cell. We will show theoretically that this case is not realistic in the steady state due to the self-adjusting effect. We assume that, for some reason, cell O_1 is more close to the central line aa', while cell O_2 is more close to the edge (see Fig. 4b). Because two cells are cramped into the space for only a single cell in equilibrium, both angles ω_1 and ω_2 are far less than their equilibrium values. Therefore, at point K, the total field is reinforced by fields E_1 and E_2, resulting in spread of cell 1 and cell 2 and consumption of aluminum at point K. However, at points c_1 and c_2, the electric field is only originated from one cell, unlike the situation at point K shown in Fig. 4b, where fields are originated from two cells. Therefore, the total fields at c_1 and c_2 are much less than their equilibrium values, leading to less consumption of aluminum at the edge. Thus, the centers of curvatures O_1 and O_2 will shift toward the central line aa'. Eventually, two cells will be merged as one single cell with a single pore, as shown in Fig. 4a.

Experimental

We use a modified two-step anodization process to fabricate a 1D nanopore array from the side of the SiO$_2$/Al/SiO$_2$/Si sandwiched structure, as shown in Fig. 1. In the first step the initial AAO is formed and then removed by chemical etching, where scallops are

created on the Al surface. In the second step, anodization continues on the same substrate to form highly ordered AAO nanopores in a steady state because the scallops serve as highly ordered seeds. All chemicals were obtained from Aldrich Chemical (St. Louis, MO) unless specified. The process is illustrated schematically in Fig. 1. First, a 100 nm layer of SiO_2 was thermally grown on an undoped 3-in. Si wafer. The wafer was previously degreased in acetone with ultrasonic agitation. Then, the film of 80–400 nm of aluminum was deposited on the oxidized Si wafers using a dc sputtering system from an aluminum source of 99.99% purity. The thickness of the aluminum film, corresponding to the number of AAO arrays (number of cells), can be accurately controlled using a quartz crystal thin-film monitor. A silicon oxide layer of ~2000 nm was then deposited on top of the aluminum layer by an e-beam evaporation apparatus from a sintered silicon oxide source of 99.95% purity. The $SiO_2/Al/SiO_2/Si$ sandwiched structure was obtained by mechanical fracture of the specimen (see Fig. 1).

After formation of the lead contact on the aluminum layer with conductive epoxy, and the subsequent sealing of the specimen except for the fractured surface with positive photoresist, a clean specimen was anodized in an oxalic acid solution of 0.2 M at room temperature at a constant applied voltage of 40 V for several minutes. Then, the anodic aluminum oxide layer was subsequently removed by dipping the anodized specimen into a mixture of phosphoric acid (6 wt %) and chromic acid (1.8 wt %) at 55°C. The second-step anodization was performed for several minutes under the same condition as the first step. Pore widening for obtaining desired dimensions was done by dipping the specimen in a 5 wt % phosphoric solution at room temperature for 10–30 min. This solution is known to dissolve the inner wall of the nanopores of the oxide films uniformly, and to enlarge the diameter of the nanopores corresponding to the etching time. The pore depth can be calculated according to the oxidation rate of aluminum. In order to dissipate the heat generated during anodization, the electrolyte solution was constantly stirred by magnetic stirrer. A regulated power supply was used to generate a dc voltage (e.g., 40 V). During pore widening, the electrochemical cell was held at room temperature (e.g., 20°C) using a controllable water bath. A field-emission scanning electron microscope (FE-SEM: JEOL JSM-6100) was used to examine all the specimens.

Results and Discussion

Fabrication of multiple arrays and a single array.— The basic assumption for fabrication of horizontal AAO arrays is that, if the electric field for anodization is in parallel with an aluminum film, the porous structure may be formed on the side of aluminum, as shown in Fig. 1. There is a correlation between the thickness of the aluminum film and number of cells for the conventional 2D AAO arrays (see Table I). For anodization in 0.2 M oxalic acid solution at 40 V, the cell size of 2D AAO arrays is 146 nm. However, there is significant discrepancy in cell and pore sizes between the low-dimension (low-D) AAO and 2D AAO arrays. The cell and pore size for our low-D AAO arrays is ~100 and ~40 nm, respectively as shown in Fig. 5 and 6, which are less than those for the conventional 2D AAO arrays. This might be caused by the reduced influence of electric field from the neighboring cells of the low-D AAO arrays. Figure 5 shows that four arrays of AAO nanopore are formed when an aluminum film with a thickness of 400 nm is used. Pores are not very ordered because the cross section shown here is near the surface. If one has an aluminum film with a thickness of 100 nm, a single array of AAO nanopores may be formed. Based on the knowledge of formation of 2D AAO arrays,[29-32] we obtained the optimal anodization parameters for formation of a 1D nanopore array after numerous sets of experiment, where a modified two-step anodic oxidation procedure was adopted, i.e., a properly short first anodization and a relatively long second anodization. In our optimal experiments, the anodization time of the first and second steps was 5 and 15 min separately at dc 40 V for 0.2 M oxalic acid electrolyte. Fig-
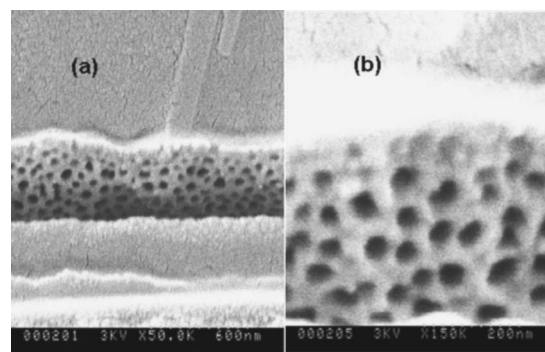

Figure 5. SEM images of four arrays of horizontal AAO nanopores formed in 0.2 M oxalic acid at 40 V for 20 min: (a) overall appearance and (b) the detailed image.

ure 6 shows the successful fabrication of a 1D AAO nanopore array horizontally aligned on the substrate. The cell size, pore size, and pore depth are 100, 40, and 500 nm, respectively. The same anodization parameters were used in the relatively thick aluminum films, 4–5 nanopore arrays shown in Fig. 5.

Evolution from multiple cells to a single cell.— Based on the above theoretical analysis, in the initial phase the nanopores nucleate at almost random locations, and pore arrangements on the surface are randomly disordered. We will examine the cross sections of samples anodized in a short time (3 min) and a longer time (15 min), representing the initial phase and the steady phase. As shown in Fig. 7a, in the initial phase pores are formed at random locations, with two or three pores in a single cell space. There are also two half-cells formed instead of a single cell, neighboring pores connected together, and pores occurring near the interfaces. Although self-adjusting begins to take place, the adjustment is not complete yet due to reduced formation time for the self-adjusting process. The higher initial growth rate also probably results in this lower degree of perfection of the structure. When the anodization is extended to 15 min (steady state), pores begin to merge to the single-cell or single-pore structure, as shown in Fig. 7b. It looks like pores are still not self-organized into a single array, because the SEM image is from the surface of the cross section, reflecting the initial growth pattern. If the initial surface is etched away, better image of a single-cell structure should appear. Figure 7c shows the results of a sample obtained using a two-step process, where the disordered part obtained in the initial anodization was etched away
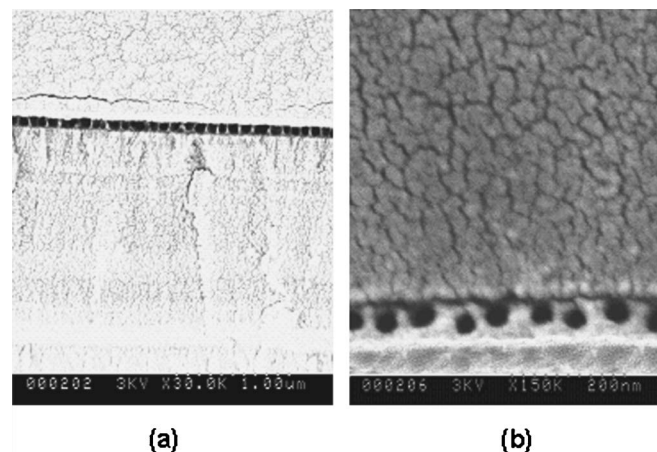
Figure 6. SEM images of a single array of horizontal AAO nanopores formed in 0.2 M oxalic acid at 40 V for 20 min: (a) overall appearance and (b) the detailed image.
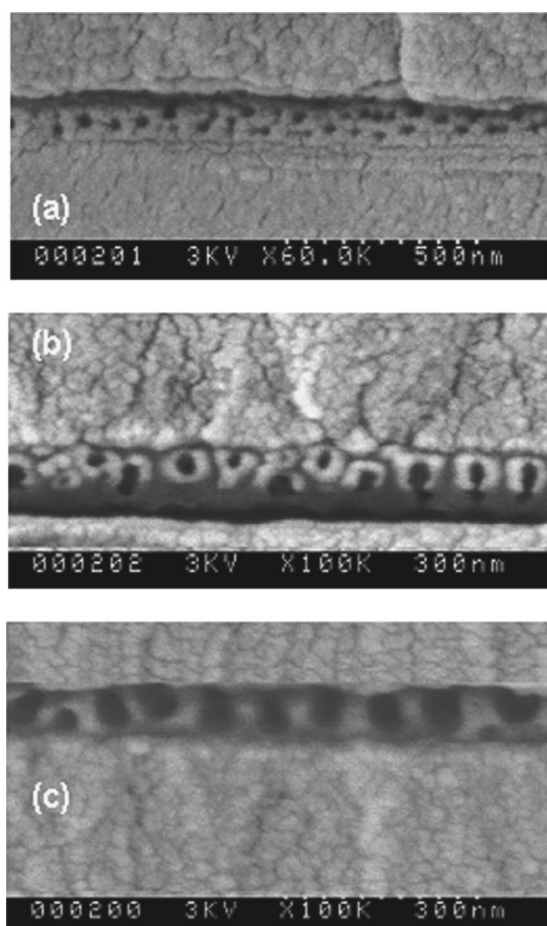
Figure 7. SEM photographs of (a) nanopore structure formed in a short time (3 min), representing a situation in the beginning of the first step where pores nucleate at random locations (the sample was anodized in 0.2 M oxalic acid at V = 40 V for 3 min); (b) nanopore structure formed by a one-step process for a longer time (15 min), representing a situation of steady state (the sample was anodized in 0.2 M oxalic acid at V = 40 V for 15 min); and (c) nanopore structure formed by a two-step process with step I lasting for 5 min and step II for 10 min, representing that more deep area was exposed.

in the first step. It can be seen that a much better image of a single array was obtained. There is a problem in viewing the SEM image if the first step lasts too long. Because the AAO is etched much faster than SiO_2, the AAO area becomes very dark if the first step lasts too long. In order to view the image properly, our first step lasted only for 5 min and the exposed cross section is still somewhat near the initial surface. If one could etch the sample further, or if the first-step anodization lasted longer, one would see a better single-array AAO nanapore.[32] These images show clearly the evolution from multiple cells to a single cell, supporting our theoretical model.

Conclusions

A simple theoretical model based on electric-field-assisted growth and dissolution of the barrier oxide has been proposed to understand the formation mechanisms of a one-dimensional AAO nanopore array. It is shown that formation of a one-dimensional horizontal nanopore array is the natural result of the self-adjusting effect of anodic oxidation. Because the electric field for anodization is in parallel with an aluminum film, the porous structure is formed on the side of aluminum. When the thickness of an aluminum film approaches the size of a single cell, a single array of nanopores evolves after anodization in a steady state for sufficiently long time. Our experimental results support the theoretical model. A well-ordered, one-dimensional nanopore array was obtained at 40 V in 0.2 M oxalic acid solution using the modified two-step anodization procedure.

References

1. S. J. Tans, A. R. M. Verschueren, and C. Dekker, *Nature (London)*, **393**, 49 (1998).
2. R. Martel, T. Schmidt, T. Hertel, and P. Avouris, *Appl. Phys. Lett.*, **73**, 2447 (1998).
3. J. T. Hu, O. Y. Min, P. D. Yang, and C. M. Lieber, *Nature (London)*, **399**, 48 (1999).
4. X. Duan, Y. Huang, R. Agarwal, and C. M. Lieber, *Nature (London)*, **421**, 241 (2003).
5. A. Bachtold, P. Hadley, T. Nakanishi, and C. Dekker, *Science*, **294**, 1317 (2001).
6. H. W. C. Postma, T. Teepen, Z. Yao, M. Grifoni, and C. Dekker, *Science*, **293**, 76 (2001).
7. T. W. Ebbesen, *Phys. Today*, **49**(6), 26 (1996).
8. W. B. Choi, D. S. Chung, J. G. S. Park et al., *Appl. Phys. Lett.*, **75**, 3129 (1999).
9. W. B. Choi, E. J. Bae, J. W. Lee, J. J. Kim, and J. O. Lee, *Appl. Phys. Lett.*, **79**, 22 (2001).
10. C. R. Martin, *Chem. Mater.*, **8**, 1739 (1996).
11. P. Hoyer, K. Nishio, and H. Masuda, *Thin Solid Films*, **286**, 88 (1996).
12. P. Hoyer, N. Baba, and H. Masuda, *Appl. Phys. Lett.*, **66**, 2700 (1995).
13. D. Crouse, L. Yu-Hwa, E. Miller, and M. Crouse, *Appl. Phys. Lett.*, **76**, 49 (2000).
14. A. Cai, H. Zhang, H. Hua, and Z. Zhang, *Nanotechnology*, **13**, 627 (2002).
15. A. J. Yin, J. Li, W. Jian, A. J. Bennett, and J. M. Xu, *Appl. Phys. Lett.*, **79**, 1039 (2001).
16. J. Liang, S. K. Hong, N. Kouklin, R. Beresford, and J. M. Xu, *Appl. Phys. Lett.*, **83**, 1752 (2003).
17. N. Kouklin, H. Chik, J. Liang, M. Izolov, J. M. Xu, J. B. Heroux, and W. I. Wang, *J. Phys. D*, **36**, 2634 (2003).
18. C. Papadopoulos, A. Rakitin, J. Li, A. S. Vedeneev, and J. M. Xu, *Phys. Rev. Lett.*, **85**, 3476 (2000).
19. F. Keller, M. S. Hunter, and D. L. Robinson, *J. Electrochem. Soc.*, **100**, 411 (1953).
20. H. Masuda, H. Yamada, M. Satoh, and T. Tamamura, *Appl. Phys. Lett.*, **71**, 2770 (1997).
21. O. Jessensky, F. Muller, and U. Gosele, *Appl. Phys. Lett.*, **72**, 1173 (1998).
22. H. Masuda, K. Nishio, and N. Baba, *Appl. Phys. Lett.*, **63**, 3155 (1993).
23. H. G. Zhang, Z. Chen, T. Li, and K. Saito, Unpublished work.
24. M. S. Hunter and P. Fowle, *J. Electrochem. Soc.*, **101**, 514 (1954).
25. G. C. Wood, J. P. O'Sullivan, and B. Vaszko, *J. Electrochem. Soc.*, **115**, 618 (1968).
26. R. Mason, *J. Electrochem. Soc.*, **102**, 671 (1955).
27. J. P. O'Sullivan and G. C. Wood, *Proc. R. Soc. London*, **317**, 511 (1970).
28. G. E. Thompson, R. C. Furneaux, G. C. Wood, and J. S. Goode, *Nature (London)*, **272**, 433 (1978).
29. J. W. Diggle, T. G. Downie, and C. W. Goulding, *Chem. Rev. (Washington, D.C.)*, **69**, 365 (1969).
30. A. Despic and V. Parkhutik, in *Modern Aspects of Electrochemistry*, J. O. M. Bokris, R. E. White, and B. E. Conway, Editors, Vol. 23, p. 401, Plenum Press, New York 1989).
31. W. C. Hu, Z. Chen, K. Saito, and C. A. Grimes, *Appl. Phys. Lett.*, **79**, 3083 (2001).
32. H. Masuda and K. Fukuda, *Science*, **268**, 1466 (1995).